# Hard carbons derived from green phenolic resins for Na-ion batteries

Adrian Beda, Pierre-Louis Taberna, Patrice Simon, Camélia Matei Ghimbeu

# Hard carbons derived from green phenolic resins for Na-ion batteries

Adrian Beda [a, b], Pierre-Louis Taberna [c, d], Patrice Simon [c, d], Camélia Matei Ghimbeu [a, b, d, *]

[a] Université de Haute-Alsace, Institut de Science des Matériaux de Mulhouse (IS2M), CNRS UMR 7361, F-68100 Mulhouse, France
[b] Université de Strasbourg, F-67081 Strasbourg, France
[c] Universite de Toulouse, CIRIMAT, UMR-CNRS 5085, F-31062 Toulouse, France
[d] Reseau sur le Stockage Electrochimique de l'Energie (RS2E), FR CNRS 3459, 80039 Amiens Cedex, France

ARTICLE INFO

ABSTRACT

Hard carbons have become recently one of the most promising classes of anode materials for sodium ion batteries (NIBs) owing to their high specific capacity and good cycling stability. Among the precursors used to prepare hard carbon, phenolic resins are of great interest due to their high carbon yield, however, their toxicity must be overcome. In this paper, we propose a green, simple and scalable procedure to obtain phenolic resins which by pyrolysis at high temperature (>1000 °C) result in eco-friendly hard carbons with low surface area, disordered structure and high carbon yield. The influence of several synthesis parameters (type of solvent, thermopolymerization/annealing temperature and gas flow) was studied to determine the impact on both phenolic resin and hard carbon characteristics. The synthesis time (12 h-3 days) was found to depend on the used solvent whereas the carbon yield (25–35%) on the cross-linking degree which could be controlled by adjusting both thermopolymerization temperature and atmosphere. The structure of the hard carbons mainly changed with the carbonization temperature (1100–1700 °C) while the texture of the material was sensitive to most of the studied parameters. Stable reversible capacity up to 270 $mAhg^{-1}$ and 100% coulombic efficiency (CE) after few cycles are obtained, demonstrating the potential for Na-ion applications.

## 1. Introduction

Carbon-based materials have been studied theoretically and experimentally for a long time as electrode materials for energy storage in applications such as supercapacitors, batteries (i.e. Li-ion batteries), fuel cells, etc. [1]. The unique combination of chemical and physical properties (abundance, low cost, superior corrosion resistance, good electronic conductivity) along with their wide availability makes carbon based electrodes promising materials for improving energy storage performances.

Li-ion batteries (LIBs) show today the best performance in terms of energy, power density and cycle stability. Negative electrode in LIBs is commonly made of graphite, which can reversibly intercalate Li-ions for thousands of cycles. However, the availability of Lithium is still an issue to solve and this is why alternatives to lithium technology are urgently needed.

One of the alternatives to LIBs can be the sodium ion batteries (NIBs). They were studied in early 1980`s in parallel with LIBs but left behind due to the breakthrough of Sony in 1991 when first commercial lithium-ion battery was released. The abundance of sodium, availability and lower costs makes sodium a promising option to replace LIBs [2]. With the new sodium cheaper ions to replace lithium and the efficient anode (graphite) we should expect new performing batteries at lower prices. However, Na ion has a larger radius than Li ion (1.02 Å *vs.* 0.76 Å) and its binding energy to graphite is weaker making the reversible intercalation difficult and thus the electrochemical performances lower than for Li-ion batteries [3]. Moreover, Na ions are mainly coordinated in octahedral sites [4] limiting the crystalline materials like graphite to provide high capacity and long cycling life. As a consequence, new potential materials to be used as anode in NIBs have been studied.

Doef et al. reported in 1993 a significant reversible capacity for carbonaceous materials when they were tested as electrode material for Na cells [5]. The electrode was prepared by pyrolysis of petroleum cokes, resulting in a soft carbon (disordered carbon but able to graphitize at high temperatures). Hard carbon represents

* Corresponding author. Université de Haute-Alsace, Institut de Science des Matériaux de Mulhouse (IS2M), CNRS UMR 7361, F-68100 Mulhouse, France.
*E-mail address:* camelia.ghimbeu@uha.fr (C. Matei Ghimbeu).

https://doi.org/10.1016/j.carbon.2018.06.036

another type of carbon materials which was highly studied during the last years. It has a disordered structure combining amorphous/graphitic domains and micropores, and it is recognized as a non-graphitizable carbon. Contrary to graphite, hard carbons do not possess a standard structural model, the so called "falling cards model" described by Dahn *et. al* being widely accepted to represent its structure [6].

Several types of precursors have been used to obtain hard carbons and they can be classified in 3 main categories, i.e., biomass waste, sugars and polymers. Hard carbons are obtained after further thermal treatment at temperatures up to 1500 °C leading to promising materials for sodium ion storage. Biomass waste (i.e., banana/pomelo/apple peels, okara, leaves, algae [7–12]) represents an important category of precursors commonly used to prepare hard carbons as detailed in a recent review [13]. The main advantage of biomass waste is their abundance which comes along with a cheap price. However, the low carbon yield, a low reproducibility due to the biowaste variety, seasonal and regional variation, limits the interest of biomass as hard carbon precursors.

Polymers and bio-polymers are another important class of precursors extensively studied as anodes for sodium ion storage. Sugars (sucrose, glucose) [14–16] and phenolic resins (resorcinol-formaldehyde gels) [17,18] along with cellulose [19], polyacrylonitrile (PAN) [20], pitch [21], sodium polyacrylate [22], etc., have been explored as carbon precursors. Unlike waste biomass where just physical parameters can be controlled, i.e., temperature, heating rate, gas flow/rate, in the case of many polymers both chemical and physical parameters can be tuned allowing different carbon structure, texture and morphology. A low carbon yield found for sugars and the toxicity issues raised by phenolic resins obtained from formaldehyde are the main disadvantages for these precursors.

Despite their toxicity, phenolic resins are interesting materials for hard carbon preparation since they deliver a high carbon yield and their characteristics can be tuned, as mention before, by both physical and chemical conditions. Want *et al.* [23] studied sodium insertion in hard carbon microspheres obtained by hydrothermal treatment of phenolic resin followed by carbonization at high temperature (880–1500 °C). The phenolic resin was obtained by mixing phenol and formaldehyde followed by addition of sodium hydroxide solution and fluorine in excess. In another study, Li *et al.* [21] used commercial phenolic resins in combination with pitch to get hard carbon materials for sodium storage. However, no details are mentioned about the composition of the phenolic resin. Remarkable electrochemical performances were reported by Ye and his team [24] when using co-doped (N and S) hollow carbon spheres (HCS) obtained from phenolic resins. The precursor is obtained by dissolving resorcinol/urea/thiourea and formaldehyde in water followed by addition of polymethyl methacrylate (PMMA) that acts as a template. A thermal treatment at 600 °C under nitrogen gas leads to the hollow nanospheres of hard carbon. Hasegawa *et al.* [25] showed promising electrochemical performances for NIBs, as well, when testing hard carbons made of macroporous phenolic precursors. In this study, sol-gel process was approached to prepare the phenolic gel, by mixing resorcinol, HCl and formaldehyde solution in presence of ethanol solvent. The carbonization temperature was varied from 800 to 3000 °C. More recently, Zhang *et al.* [26], prepared hard carbons from a mixture of phenolic resin and sucrose. By changing the mass ratio of sucrose/resin, different carbon materials were obtained under thermal treatment at temperatures between 1000 and 1600 °C. However, the resin is made of phenol and formaldehyde, as in the previous studies.

As highlighted in these works, most of phenolic resins used to obtain hard carbons are based on phenol/formaldehyde which is highly toxic for human and environment. To the best of our knowledge, there is no paper presenting alternatives to obtain green phenolic resins for hard carbon preparation. In this work we propose a simple, versatile and green synthesis approach to obtain hard carbon materials with tunable properties (porosity and microstructure). Phloroglucinol and glyoxylic acid, both extracted from natural sources [27,28] are simply dissolved in water/ethanol solvents at room temperature allowing the formation of a green phenolic resin gel. Thermal annealing of such resins at high temperature resulted in hard carbon materials with tunable features (high disorder degree, large interlayer spacing, low specific surface area etc) for Na-ion energy storage. The influence of synthesis parameters on the obtained phenolic resin and hard carbon characteristics was studied in detail by several analyses techniques. Selected materials were tested for Na-ion batteries showing a reversible capacity of around 270 $mAh \cdot g^{1}$, which is relatively stable over cycling and a high Coulombic efficiency of 100% after few cycles.

## 2. Materials and methods

### 2.1. Material synthesis

Phloroglucinol (1,3,5-benzentriol, $C_6H_6O_3$) and glyoxylic acid monohydrate ($C_2H_2O_3 \cdot H_2O$) were purchased from Sigma-Aldrich and used as received without any further purification. Ethanol ($C_2H_6O$) and distilled water were used as solvents.

The hard carbon materials (HC) were synthesized by a sol-gel approach followed by thermopolymerization at a low temperature to cross-link the resin and thermal treatment (TT) at high temperature to decompose and carbonize the resin.

The synthesis procedure is very simple, scalable and consists in the dissolution of phloroglucinol (3.26 g) and glyoxylic acid (3.6 g) at room temperature in 40 mL of solvent (water, ethanol or the mixture of both - 1:1 ratio). Next, the solution is placed on an oil bath to ensure constant temperature (25 °C) for a certain period of time favoring the polymerization process and the formation of a phenolic resin gel (12 h–3 days, depending on the solvent used). Once the gel formed, it is placed in an oven and dried in air at a temperature up to 150 °C for ~12 h. Further, we will refer to this step as thermopolymerization (TP). For the final step, the cross-linked resin was thermally treated (TT) at 1300 °C under Ar (15L/h). The obtained material was manually grinded for further characterizations. The entire procedure is schematically presented in Fig. 1.

Several parameters were investigated by changing one parameter at the time, the other being kept constant, i.e., the solvent type (ethanol, water, ethanol/water mixture), thermopolymerization temperature (25 to 150 °C), thermopolymerization atmosphere (air, argon, freeze–drying, simple vacuum) and thermal annealing temperature (1100 to 1700 °C). The detailed synthesis parameters along with the sample denomination are presented in Table 1.

### 2.2. Material physico-chemical characterization

Several characterization techniques were used to analyze both the phenolic resin and the hard carbon material. Starting with the phenolic resin, its structure was studied by $^{1}H$ and $^{13}C$ cross-polarization magic angle spinning (CP/MAS) solid state NMR. The spectra were obtained at the frequency 100.6 and 400.13 MHz, on a Bruker Avance 400 NMR spectrometer. Chemical surface of the phenolic resin was characterized using a Bruker Fourier transform infrared spectrometer model IFS66/S with a MCT detector, 4000-400 $cm^{-1}$ spectral range. Thermo-gravimetric analysis was performed to study the mass loss of the resin by heating at a temperature up to 1300 °C at 5 °C/min under nitrogen atmosphere


**Fig. 1.** Environmentally friendly synthesis procedure developed to prepare the hard carbon materials using phloroglucinol/glyoxylic acid resin. (A colour version of this figure can be viewed online.)

**Table 1**
Synthesis conditions used to prepare hard carbon materials.

| Sample name | Solvent | TP temp. (°C) | TP atm. | TT (°C) |
|---|---|---|---|---|
| HC ethanol | ***Et-OH*** | 80 + 150 | Air | 1300 |
| HC mixture | ***Et-OH/$H_2O$*** | 80 + 150 | Air | 1300 |
| HC water | ***$H_2O$*** | 80 + 150 | Air | 1300 |
| HC air | Et-OH | 80 + 150 | ***Air*** | 1300 |
| HC argon | Et-OH | 80 + 150 | ***Argon*** | 1300 |
| HC freeze drying | Et-OH | – | ***Freeze-drying*** | 1300 |
| HC vacuum | Et-OH | 80 + 150 | ***Vacuum*** | 1300 |
| HC 25 °C | Et-OH | ***25*** | Air | 1300 |
| HC 80 °C | Et-OH | ***80*** | Air | 1300 |
| HC 150 °C | Et-OH | ***150*** | Air | 1300 |
| HC 80 + 150 °C | Et-OH | ***80 + 150*** | Air | 1300 |
| HC 1100 °C | Et-OH | 150 | Air | ***1100*** |
| HC 1300 °C | Et-OH | 150 | Air | ***1300*** |
| HC 1500 °C | Et-OH | 150 | Air | ***1500*** |
| HC 1700 °C | Et-OH | 150 | Air | ***1700*** |

Italic text denotes the modified synthesis parameter.

(Mettler-Toledo TGA 851e). Temperature-programmed desorption (TPD) analysis was performed in a "homemade" vacuum system equipped with a mass spectrometer [29]. The samples were heat-treated up to 950 °C at a heating rate of 5 °C $min^{-1}$. The gas phase was quantitatively analyzed during the experiment by the mass spectrometer. Prior the analysis, the mass spectrometer was calibrated using: $H_2$, $H_2O$, CO, $N_2$, $O_2$ and $CO_2$ gases.

The structure of carbon materials was studied by Raman and X-ray powder diffraction (XRD). Raman measurements were performed at room temperature using a LabRAM BX40 (Horiba Jobin-Yvon) spectrometer equipped with He-Ne excitation source (532 nm wavelength). XRD analysis was performed using a Bruker D8 Advanced diffractometer with flat-plate Bragg-Brentano θ-θ geometry.

Textural properties of the hard carbon materials were investigated with a Micromeritics ASAP 2420 machine using $N_2$ gas as adsorbate (77 K) and a Micromeritics ASAP 2020 instrument using $CO_2$ adsorbate (273 K). Previously, the samples were out-gassed for 12 h at 300 °C, under vacuum, on the degassing ports and additional, for another 2 h on the analysis ports. The BET (Brunauer–Emmett–Teller) specific surface area (SSA) was determined from the linear plot in the relative pressure range 0.05–0.3, whilst the pore size distribution (PSD) was calculated from both $N_2$ and $CO_2$ adsorption isotherms using the NLDFT (non local density functional theory) standard model for carbon materials carry out by SAIEUS software [30]. The morphology of the hard carbon materials was studied by high resolution transmission electron microscopy (HRTEM) and selected area electron diffraction (SAED) with a JEOL, ARM-200F model instrument operating at 200 kV.

### 2.3. Material electro-chemical characterization

The electrochemical tests were done using Swagelok cells. The electrodes were obtained by mixing the hard carbon active material with polyvinylidene fluoride (PVdF) and carbon black acetylene with a mass ratio of 70:10:20. All the components were mixed in presence of N-methyl-2-pyrrolidone (NMP) and the obtained slurry was coated by doctor blade on Al foil. The obtained electrode was dried at 80 °C overnight under vacuum. Before using, it was punched to get the desired size. The active mass loading for the obtained electrodes is between 1.4 and 2 mg $cm^{-2}$. As counter/reference electrode sodium metal was used while the electrolyte was 1M solution of $NaPF_6$ in ethylene carbonate (EC)/dimethyl carbonate (DMC), 1:1 in volume.

Electrochemical performances were measured using a Bio-Logic cycler. Galvanostatic charge-discharge tests were conducted at a constant current <I>. First the discharge is performed at a negative current in the range 2V-0.01 V. The current was then reversed to charge the cell to the same maximum cell voltage of 2 V. Cyclic voltammetry was performed in a voltage window between 0.01 and 2 V at scan rates of 0.2 mV $s^{-1}$. All the experiments were conducted at room temperature.

## 3. Results and discussion

A series of samples was prepared in order to understand how the experimental parameters impact the hard carbon characteristics (Table 2). Both phenolic resins and hard carbon materials have been studied in detail.

### 3.1. Hard carbon characterization

XRD and Raman techniques were used to obtain information about the carbon structure when changing different synthesis parameters (solvent, thermal polymerization temperature/atmosphere and annealing temperature). The XRD patterns of the hard carbon materials are characterized by three broad peaks observed at 22.4°, 43.5° and 80° which correspond to (002), (100) and (110) diffraction planes of graphite (Fig. 2a). However, the broad shape of the peaks suggests a low graphitization degree. The thickness of the graphitic domains (Lc) was calculated using the Scherrer equation and the size was found to be close to 1 nm (for the materials treated at 1100–1300 °C), indicating that they are composed of 2–3 layers of graphene. These features are specific for hard carbon materials

**Table 2**
Carbon yield, structural and textural characteristics of hard carbon materials prepared in different conditions.

| Changed Parameter | Sample name | C yield wt% | $d_{002}$ Å | $I_D/I_G$ | $N_2$ SSA $m^2\ g^{-1}$ | $CO_2$ SSA $m^2\ g^{-1}$ |
|---|---|---|---|---|---|---|
| Solvent | HC ethanol | 32.8 | 3.98 | 1.29 | 7,9 | 116.3 |
| | HC mixture | 31.6 | 4.02 | 1.17 | 54,3 | 291.3 |
| | HC water | 31.0 | 3.98 | 1.3 | 72,4 | 219.96 |
| TP atmosphere | HC air | 32.7 | 3.98 | 1.29 | 7.9 | 116.3 |
| | HC argon | 33.5 | 3.92 | 1.28 | 4.8 | 52.8 |
| | HC freeze drying | 24.9 | 3.9 | 1.33 | 13.5 | 87.5 |
| | HC vacuum | 34.6 | 3.95 | 1.33 | 8 | 130.4 |
| TP temperature | HC 25 °C | 21.9 | 3.94 | 1.26 | 80.6 | 148.2 |
| | HC 80 °C | 34 | 3.90 | 1.28 | 5.5 | 55.97 |
| | HC 150 °C | 34.3 | 3.87 | 1.26 | 6 | 79.7 |
| | HC 80 + 150 °C | 32.9 | 3.98 | 1.29 | 7.9 | 116.3 |
| Carbonization temperature | HC 1100 °C | – | 3.96 | 1.43 | 36 | 273.3 |
| | HC 1300 °C | – | 3.87 | 1.29 | 6 | 79.7 |
| | HC 1500 °C | – | 3.79 | 1.26 | 4.2 | 7.5 |
| | HC 1700 °C | – | 3.7 | 1.26 | 3.7 | 20.8 |

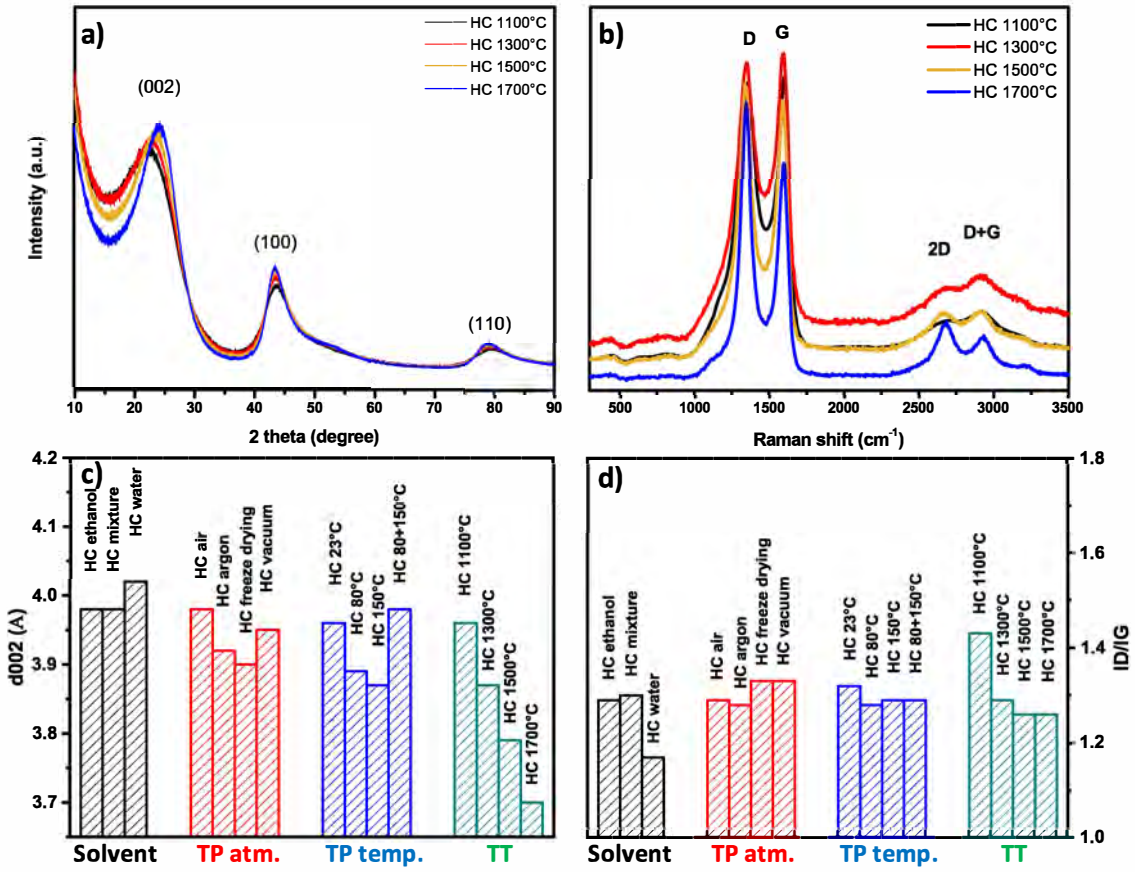


**Fig. 2.** a) XRD and b) Raman spectra of hard carbon materials thermally treated between 1100 °C and 1700 °C; Influence of synthesis parameters on materials characteristics: c) d-spacing; d) graphitization degree. (A colour version of this figure can be viewed online.)

with a disordered structure and, at the same time, a certain degree of graphitization.

The derived hard carbons obtained by treatment at 1300 °C show three characteristic XRD peaks placed at the same two theta positions (22.4°, 43.5° and 80°) no matter the solvent or thermo-polymerization temperature/atmosphere. As result, the d-spacing values obtained are almost identical, 4 Å (Fig. 2c). On the contrary, for hard carbons prepared at annealing temperature between 1100 and 1700 °C clear changes can be seen in the XRD spectra (Fig. 2a). The (002) peak position shifts to higher two theta angles and the intensity increases with the increase of the temperature. Consequently, the d-spacing decreases from around 4 Å at 1100 °C to 3.7 Å at 1700 °C. This is related to the stacking of disordered graphene sheets at higher temperature, therefore increasing the graphitization level. The increase in the graphitization level is confirmed, as well, by the evolution of (110) plane which is characteristic for graphitic structures.

This tendency is confirmed by HRTEM and SAED (Fig. S1, Supporting Information). Agglomerations of curved graphene layers with random orientation, similar to the "card house" model of

disordered hard carbons proposed by Dahn and co-workers [6] could be seen for all samples. The internal organization of graphene layers is higher with the increase of temperature (from 1100 to 1700 °C) and it is confirmed by the Lc value that increases from 1 nm to more than 2 nm, corresponding to 4 to 5 graphene layers stacked together at 1700 °C. Selected area electron diffraction confirms, as well, graphitization improvement with temperature since the diffraction rings become more defined at higher temperature.

Raman analysis was used to get additional information about the structure of hard carbon materials. All the spectra show two intense and sharp peaks in the range: 1100-1700 $cm^{-1}$ (Fig. 2b). The first peak at 1343 $cm^{-1}$ corresponds to the defect induced D-band while the second one is correlated to crystalline graphite G band (1596 $cm^{-1}$). By determining the ratio between the intensity of D and G bands ($I_D/I_G$) one can quantify the degree of structural disorder. The D band has low intensity in well organized (graphitized) materials but for this series of hard carbons the peak is more intense than the G peak, indication of disordered structure. Additional, two broad peaks can be identified in the region 2500-3000 $cm^{-1}$ corresponding to 2D and D + G bands. The D + G band was reported as a defect activated process for an elastic scattering event to provide momentum conservation in the Raman process (as the D band is) while the 2D band shows information on the degree of graphitization in the material, this peak being characteristic for bulk graphite. Such peak become well visible and its intensity increases with the annealing temperature, confirming the formation of graphitised domains in the materials besides the disordered domains.

When different solvents and thermopolymerization temperature/atmospheres were approached, the Raman spectra exhibited similar shape with small differences in which concerns the intensity of D and G bands. This aspect is reflected by the small variation of $I_D/I_G$ ratio (between 1.17 and 1.3), values that indicates a high disorder degree (Fig. 2d). However, when the phenolic resins were pyrolysed at different temperatures, the intensity of G bands starts to decrease with the increase of temperature, the $I_D/I_G$ ratio decreases while the full-width decreases as well. Moreover, the 2D band which is correlated to the graphitization level becomes sharper when increasing the temperature from 1100 to 1700 °C (Fig. 2b). This is in good agreement with the previous results found for XRD and TEM analyzes indicating better structural organization with the increase of the temperature.

The porosity of the obtained hard carbon materials was studied by nitrogen adsorption-desorption and $CO_2$ adsorption isotherms. Type I isotherms (Fig. 3a) could be found for all the hard carbons typical for materials with micro and ultramicroporous structure for which pore filling occurs at relative pressure below 0.1 and the process is complete at a partial pressure of around 0.5. However, for many materials, the adsorbed volume at low pressure is very small indicating rather non-porous materials. Desorption process is not complete and a possible explanation is that some $N_2$ molecules are trapped inside the pores, phenomenon observed when the pores present an ink-bottle neck like shape [31].

Fig. 3c shows the nitrogen BET SSA results of the hard carbons obtained by varying the synthesis parameters. Textural properties of the hard carbon material are mainly affected by the solvent used and thermopolymerization step. When different solvents were

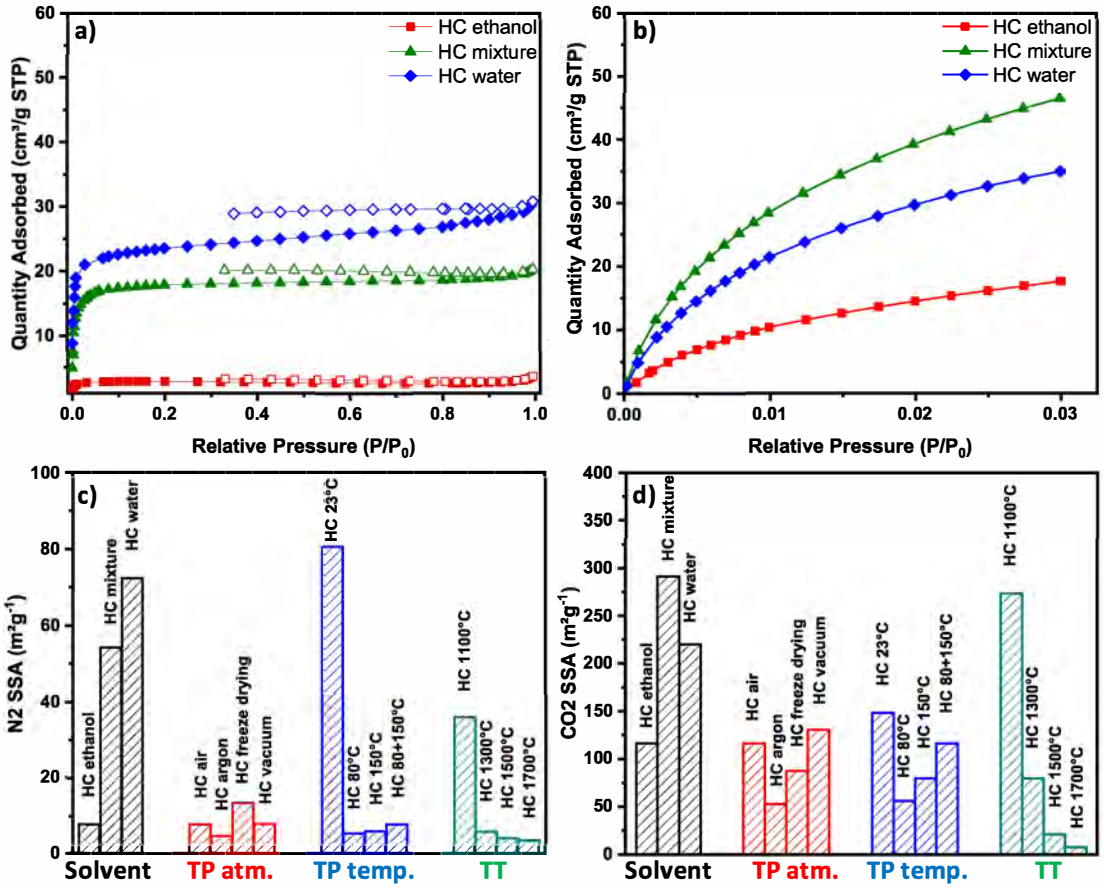


**Fig. 3.** a) Nitrogen adsorption/desorption isotherms and b) $CO_2$ adsorption isotherms of hard carbon materials obtained by using different solvents. Influence of synthesis parameters on carbon characteristics: c) $N_2$ BET SSA and d) $CO_2$ BET SSA. (A colour version of this figure can be viewed online.)

used, it was found that HC water adsorbs seven times more nitrogen that HC ethanol. This lead to a BET specific surface area of 72.4 $m^2 g^{-1}$ (HC water) comparing to 7.9 $m^2 g^{-1}$ (HC ethanol), Table 2. Thermopolymerization at room temperature gives higher SSA (80.5 vs. ~8 $m^2 g^{-1}$) than the samples dried at temperatures between 80 and 150 °C. Different thermopolymerization atmospheres do not bring differences on the material texture (see Table 2, Fig. 3c). When varying the carbonization temperature, the BET values constantly decrease with the increase of temperature, i.e., 36 $m^2 g^{-1}$ for the sample treated at 1100 °C and between 6 and 3.7 $m^2 g^{-1}$ when treating up to 1700 °C.

$CO_2$ adsorption analysis was performed, as well, to get more information about the existence of ultramicroporosity in the materials (Fig. 3b). Ultramicropores cannot be accessed by $N_2$ molecules, but it is possible by using $CO_2$ gas [13]. The results showed that the specific surface area determined by $CO_2$ adsorption is significantly higher compared to $N_2$ BET SSA (i.e. 273 $m^2 g^{-1}$ vs. 36 $m^2 g^{-1}$ for HC1100 °C) suggesting an extra-porosity coming from small size pores (<0.7 nm) which are not accessible by $N_2$ molecules, but accessible when using $CO_2$ gas. The results obtained for the evolution of $CO_2$ SSA of the materials are similar to the ones observed for $N_2$ SSA, i.e., the highest SSA (291.3 $m^2 g^{-1}$) for HC water while the lowest (116.3 $m^2 g^{-1}$) for HC ethanol (Fig. 3d).

Pore size distribution confirms the results obtained by $N_2$ and $CO_2$ adsorption and as example, the plots for pore size distribution of hard carbon obtained by using different solvents are presented (Fig. S2, Supporting Information). Microporosity (<2 nm) is revealed by nitrogen pore distribution with a size centered at around 1.2 nm. However, pore size distribution determined using the $CO_2$ adsorption results showed a higher volume of pores (10 times higher than $N_2$ PSD). The pores are of ultramicroporosity scale with the size centered of around 0.6 nm. It is worth mentioning here that the pore volume is 5–6 times higher for the materials obtained by using water as solvent (solely or as mixture with ethanol) than the materials prepared with ethanol solvent.

As seen by the analyses described before, the structure and the texture of the materials is influenced strongly by the initial preparation conditions of the phenolic resin and by the annealing temperature. In order to get more insights in the formation of the hard carbon, the phenolic resins were studied in detail.

### 3.2. Phenolic resin characterization

Three of the four parameters studied (the solvent, TP temperature and TT) affected the characteristics of hard carbon materials. As we have already seen, hard carbon materials with different properties (SSA, d-spacing, structure, etc.) were obtained by varying the experimental conditions and this may be associated to the modifications induced on phenolic gel characteristics. Thus, it is very important to study the formation of phenolic resin polymer.

The parameter we will discuss in detail is the influence of solvent since it induce important differences in material porosity. It was found that each solvent used requires different time for phenolic resin gel formation: 12 h when water is used as solvent, 24 h for water-ethanol mixture and 3 days for ethanol. This time can be correlated to some extent to the content of −OH groups. Water has a higher concentration of −OH groups and thus more protons can be formed while the concentration of hydroxyl groups is lower for ethanol. The increase of the pH favors the formation of substituted phloroglucinol molecules and thus the formation of polymer molecules. Visually and mechanically speaking, the three resin gels obtained are similar but this is not enough to confirm that the time approached for each case lead to materials with a similar crosslinking degree.

FT-IR was performed to get information on the chemical surface of the phenolic resins synthesized using different solvents. The observed peaks for the resins prepared at room temperature (25 °C) could be labeled to chemical bonds of precursors (-OH, -COOH), cross-linked precursors (C=O, C-O-C,) or solvents (-$CH_2$, -OH). Only small difference can be seen from the spectra of the three samples (see SI Fig. S3). The most important difference is the intensity of the signals obtained. When ethanol was used as solvent the signal is slightly higher otherwise, similar vibration bands at similar wavenumber were observed.

A much clear difference could be seen when comparing the three spectra of resins dried at 25 °C with the one dried at 80 °C (black curve, Fig. S3), the later one presenting a lower intensity of all peaks. When the resin gel is dried at room temperature, the intensity of the peaks is higher since the reactions between the compounds are at an early stage with a high amount of solvent still present in the structure (removable at higher temperatures) and intermediate compounds that are not yet cross-linked. At 80 °C, the reaction between phloroglucinol and glyoxylic acid is more advanced and the polymerization degree is higher, reason why the vibration bands decrease in intensity.

These observations suggest that ethanol-derived resins are less cross-linked taking into account that the intensity of several functional groups is higher (O-H, -COOH, -C-O-, etc), therefore not involved in cross-linking. Another important finding is that the thermopolymerization increases the cross-linking degree of the resins. This observation may be linked with the porosity of the obtained carbons which were more porous when water is used (more cross-linked).

$^{13}C$ and $^{1}H$ NMR were used to analyze the structure/polycondensation degree of the phenolic resin (Fig. 4a and b) obtained in presence of different solvents (ethanol, water or the mixture of both). $^{13}C$ CP-MAS NMR spectra show several chemical shifts in the range 200-0 ppm with the main resonances rather similar for each sample. The peaks correspond to carbon atoms from different initial precursors species as well as from cross-linked products formed by the polymerization reaction between glyoxylic acid and phloroglucinol in the presence of solvent as identified elsewhere [32,33]. The chemical shift at 176.9 ppm corresponds to the carbon atoms of carboxylic group (C=O) present in glyoxylic acid. Next chemical shift present at 154 ppm is due to the unsaturated aromatic carbon bonded to oxygen in phloroglucinol. The intensity of the peak is lower for the sample obtained with water as solvent which means that the amount of free (un-reacted) phloroglucinol is lower comparing with the other two samples.

The two resonances at 106.7 and 99.9 ppm associated with the unsaturated aromatic carbon bonded with the C atom of the trihydroxy phenylacetic acid and the saturated carbon atoms. The peak corresponding to the saturated carbon atoms is just a small shoulder in the well defined resonance at 106.7 ppm, meaning that the amount of these species is low and mixed with trihydroxy phenylacetic acid due to incomplete reaction with the glyoxylic acid. Next, there is a series of three low intense peaks at 73.8, 63.5 and 58.7 ppm respectively, which might be assigned to intermediate products of polymerization in low amounts which are very sensitive to the solvent used (the sample prepared in presence of water shows just a broad and small peak). The last chemical shift that is present for all the samples at 40.3 ppm can be associated with the carbon from lactone bridges that connect the phloroglucinol rings. Two sharp peaks at 17.1 and 14.1 ppm are observed for the samples prepared with ethanol as solvent correlated to methyl groups.

$^{1}H$ NMR was used to study further the structure of the phenolic resins. Three chemical shifts were identified at 5.5 ppm, 3.2 ppm and 0.63 ppm, respectively (Fig. 4b). One intense signal could be identified at 5.5 ppm and it is correlated to the protons from

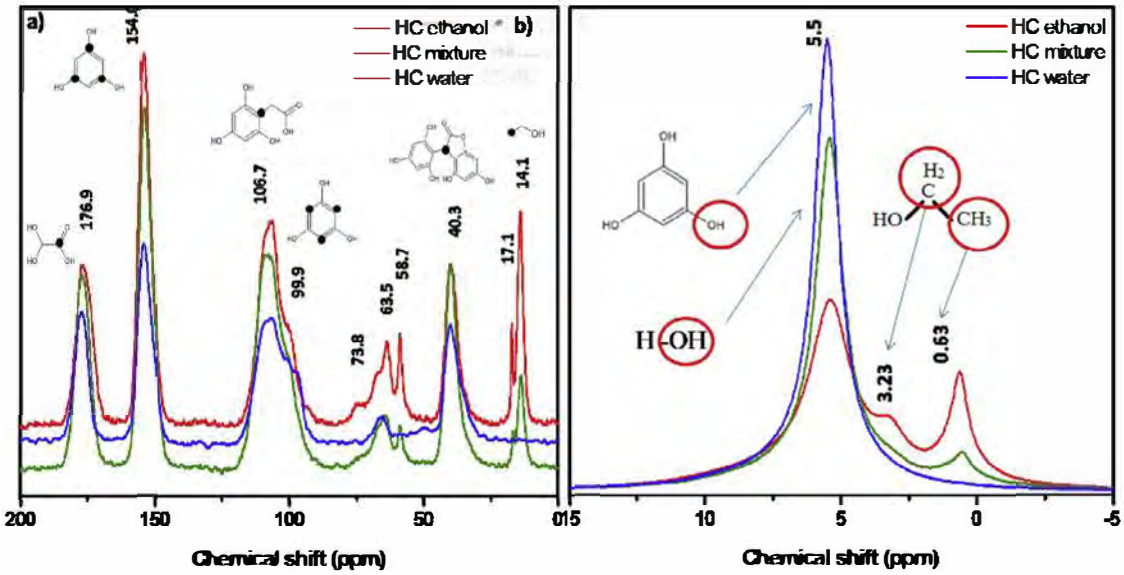


**Fig. 4.** $^{13}C$ CP-MAS NMR (a) and $^{1}H$ NMR (b) spectra of the phenolic resins synthesized in presence of different solvents and corresponding chemical structures associated with each peak (*in-set*). (A colour version of this figure can be viewed online.)

phloroglucinol —OH groups as well as to the water —OH groups. This peak varies with the solvent used having the highest intensity for water sample and the lowest one for ethanol sample. The low intense peak at 3.2 ppm and the peak from 0.63 ppm are related to protons from methylene (-$CH_2$) and methyl (-$CH_3$) groups, respectively and are observed just for HC ethanol materials. However, it is difficult to discriminate between the contribution of water and phloroglucinol to the peak intensity meaning that we cannot correlate peak intensity with cross-linking degree. Moreover, there is a difference between the broadness of the three peaks. Ethanol sample exhibits the largest peak due to a lower cross-linking degree which is in agreement with the results obtained from $^{13}C$ CP-MAS NMR.

Thermal analysis techniques (TGA and TPD-MS) were employed to study the transformation of phenolic resin into hard carbon. During the thermal treatment process which is performed under inert atmosphere (argon flow), volatiles such as $H_2O$, CO, $CO_2$, $H_2$, etc, are removed from the composition of the phenolic resin. More precisely, thermal fragmentation and decomposition of the polymeric structure with formation of glassy carbon structure occur as result of the condensation of aromatic molecules and the volatilization of low molecular weight species [34]. The impact of experimental parameters on the carbon formation was evaluated, starting with the thermopolymerization temperature (Fig. 5a).

Three decomposition domains were identified as follow: the first one between 30 and 250 °C, it is related to solvent removal as well as water molecules removal which result from polycondensation reactions due to cross-linking of phenolic resin. TPD-MS analysis gives more information about the nature of the chemical species produced during the polymer precursor transformation into carbon. Gases desorption profiles evolution over temperature for one typical phenolic resin can be seen in Fig. S4, Supporting Information. At low temperature (<250 °C), water is desorbed along with small amounts of $CO_2$ and $H_2$. $CO_2$ gas formation may be due to the decomposition of acidic groups (i.e. carboxyl, -COOH) and/or anhydride groups derived from glyoxylic acid. During the first step, between 8 and 30% mass loss occurs, depending on the used synthesis conditions. The second domain between 250 and 500 °C can be attributed to different species evolved during the thermal decomposition of phenolic resin, corresponding to a mass loss between 45 and 57%. TPD-MS analysis shows three intense peaks that correspond to $H_2O$, CO and $CO_2$ gas release. Small amounts of $H_2$ are released as well. With the increase of temperature, structural water is produce from the reactions between neighboring carboxylic groups (-COOH) of glyoxylic acid. This chain of reactions implies the cross-linking of the phenolic resin as well as the material carbonization. The lactone decomposition results in CO gas while anhydrides groups (which were formed at low temperature, during the first step) decompose at higher temperatures (~360 °C) with formation of water, CO and $CO_2$. The last domain, which starts from 500 °C up to 1300 °C, can be correlated to the removal of oxygen functional groups and structural organization of the carbon. At high temperature the quantity of $H_2$ desorbed is the most significant as shown by TPD-MS results and a broad and low intense peak can be seen. $H_2$ desorption occurs due to the internal organization of carbon which involves C-H bond cleavage. Water and CO are desorbed as well in low amounts.

TGA results showed a total mass loss between 65 wt% and 80 wt % for the different samples. When the resin gel is dried at room temperature, the obtained precursor gives around 13% lower carbon yield (21% *vs.* 34% at 1300 °C) compared to gels dried at a higher temperature (Fig. 5b), associated with a faster degradation rate due to a lower cross-linking degree. The derivative weight loss plot (black dotted line Fig. 5a) shows a narrow and intense peak with maximum at 75 °C for the room temperature-dried sample. Considering these results, a thermopolymerization temperature of 80 °C leads to a high-enough crosslinking degree to obtain a high carbon yield.

When the influence of solvent was studied, only small differences from the TGA plots could be seen between the three samples and similar final carbon yield of about 31% was obtained (see Table 2). TGA results showed that all the parameters give similar yields except freeze drying and room temperature samples with efficiency between 22 and 25%.

### 3.3. Hard carbon electrochemical performances

To show the interest of these materials, we have tested a series of hard carbons (influence of solvent) as anodes for Na-ion

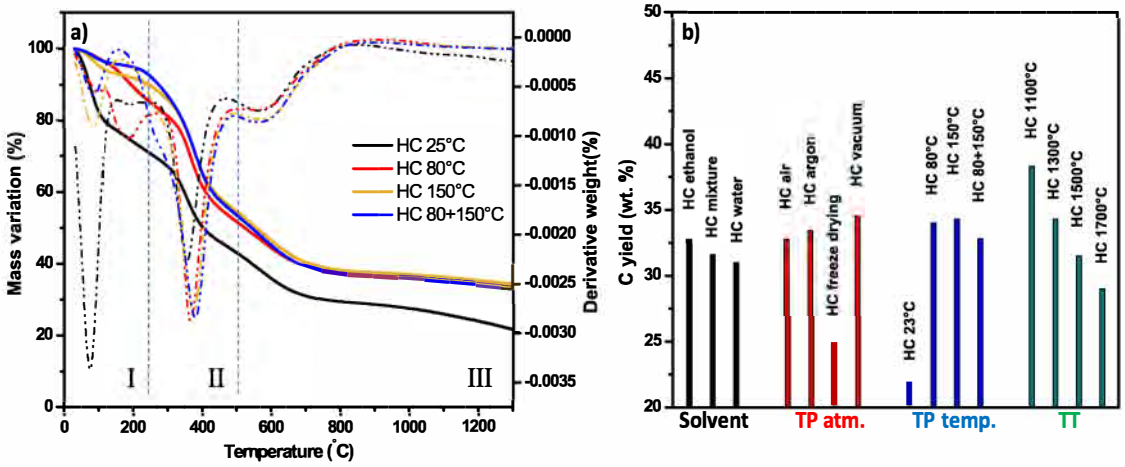


**Fig. 5.** a) TGA/DTG spectra of phenolic resin gel: decomposition steps; b) Influence of synthesis parameters on the carbon yield (%). (A colour version of this figure can be viewed online.)

batteries. The first description of sodium ion storage in hard carbon anodes was reported by Stevens and Dahn in 2001 [35] and widely accepted for several years. They state that Na-ions are first inserted within the graphene layers at high voltage while at low voltage (0–0.2 V) adsorption into the pores occurs. However, a more recent study published by Ghimbeu *et al.* [13], propose a different mechanism which attributes the slope region in the range 0.2–2 V to sodium ion insertion in the porosity, presence of defects and functional groups while the plateau at low voltage is linked to sodium intercalation. This new mechanism is rather more accepted now as revealed by the review article of Bommier [36] which gather several recent experimental and theoretical works. In order to facilitate Na ions storage, materials with a large d-spacing, low specific surface area (since high SSA favors the solid electrolyte interphase (SEI) formation) and presence of defects are desired, as presented by Sawicki and Shaw [37]. Taking into consideration all these aspects, three materials obtained from different solvents, thermally treated at 1300 °C, were selected for performing electrochemical tests (interlayer distance ~ 4 Å, BET SSA between 8 and 80 $m^2 g^{-1}$, $I_D/I_G$ ~ 1.3). Fig. S5 shows an example of cyclic voltammetry (CV) results. In the first cycle, CV curve shows a broad cathodic peak at around 0.25 V due to the SEI layer formation [20]. This phenomenon seems to occur in the subsequent cycles as well but the irreversible compounds formation is less significant. At low voltage (near 0 V), two redox peaks can be identified, similar with the behavior observed in lithium ion batteries. These two peaks are attributed to the reversible insertion-extraction of Na ions within graphene-like layers. The electrochemical signature of the hard carbon material is then compatible with Na-ion applications. The first cycles of galvanostatic discharge-charge profiles at a current

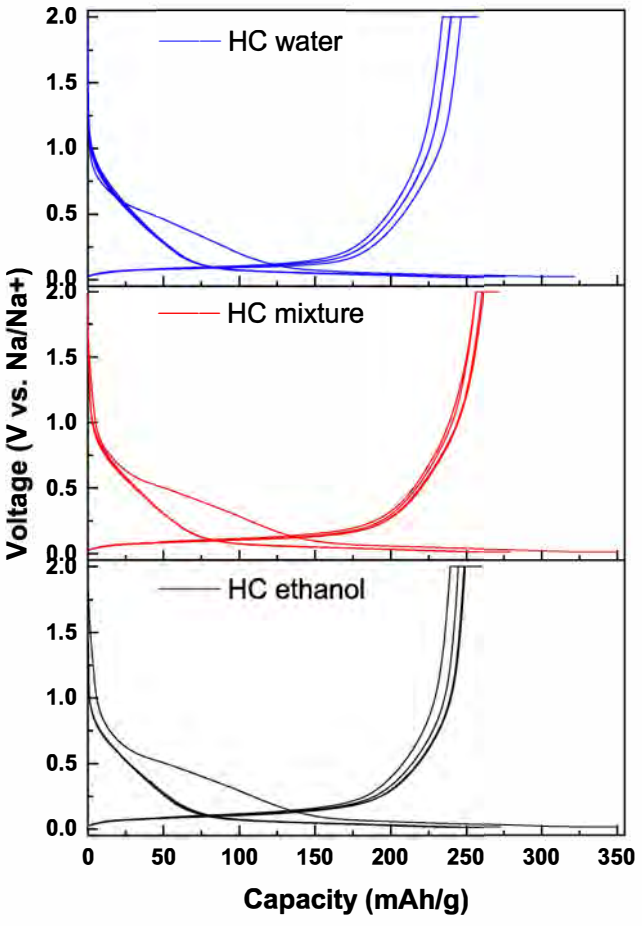


**Fig. 6.** Galvanostatic discharge-charge profiles of HC ethanol (bottom), HC mixture (middle) and HC water (top) at current density of 37.2 mA $g^{-1}$. (A colour version of this figure can be viewed online.)

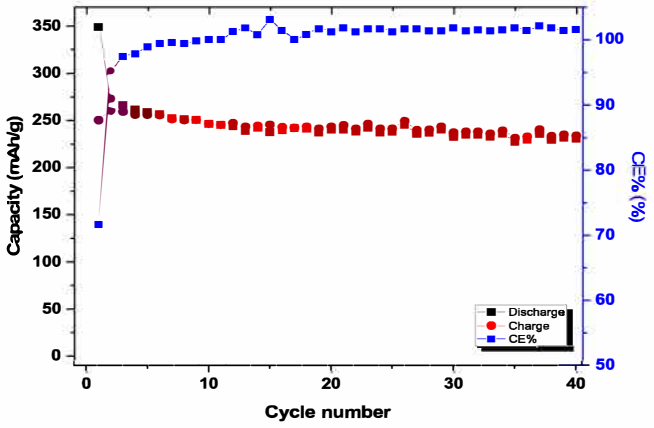


**Fig. 7.** Long term cycling stability and CE% of hard carbon sample at current rate: C/10. (A colour version of this figure can be viewed online.)

**Table 3**
Literature data on phenolic resins derived hard carbons electrochemical performances. Details on resin preparation and main characteristics are presented as well.

| Precursor | T pyrolysis (°C) | $d_{002}$ (Å) | $N_2$ BET ($m^2 \cdot g^{-1}$) | iCE (%) | Rev cap. (mAh/g) | Ref. |
|---|---|---|---|---|---|---|
| Pitch: phenolic resin (1:1) | 1400 | 3.77 | 2.1 | 86 | 259 | [21] |
| Phenol/formaldehyde resin | 1250 | 3.89 | 219.5 | 60.2 | 311 | [23] |
| Resorcinol/ formaldehyde resin | 1200 | 4.14 | 420 | 86 | 200 | [25] |
| Phenol-formaldehyde resin: sucrose (1:2) | 1200 | 3.95 | 4.5 | 83 | 295 | [25] |
| Phloroglucinol-glyoxylic acid resin | 1300 | 3.98 | 7.9 | 76 | 270 | This work |

density of 37.2 mA $g^{-1}$ are presented in Fig. 6. At the first cycle, the materials deliver a discharge specific capacity of about 350 $mAhg^{-1}$ for HC ethanol and HC mixture and slightly lower for HC water (325 $mAhg^{-1}$), probably due to its higher specific surface area. However, the maximum charge capacity reaches 270 $mAhg^{-1}$ for HC mixture (250 $mAhg^{-1}$ for the other materials). This ~20% irreversible capacity can be explained by the SEI formation, also observed in CVs, irreversible intercalation or/and sodium ion trapping into the porosity. Starting with the second cycle, the SEI layer is almost stable and only a low irreversible capacity is observed (<20 $mAhg^{-1}$) which continuously diminishes in the following cycles. However, this is an initial characterization and a more in-depth study is under investigation.

Since the three materials exhibits rather similar capacities, long term performances for only one sample (HC ethanol) are presented in Fig. 7.

The analysis was done at C/10 rate, where 1C was considered 372 $mAg^{-1}$ (in reference to Li ion intercalation into graphite electrodes). The specific discharged and charge delivered by the electrode in the first cycle is 350 and 250 $mAhg^{-1}$, respectively, corresponding to an initial Coulombic efficiency (CE) of 71.6%. In the subsequent cycles, the CE significantly increases and 100% efficiency is reached starting with the 5th cycle. The anode material shows relatively stable capacity in the first 40 cycles with local fluctuations.

Comparable performances have been reported in literature for hard carbon anodes derived from toxic resins in similar TT conditions (1200–1400 °C) and exhibiting similar characteristics, i.e. $d_{002}$ ~ 4 Å and SSA <8 $m^2 g^{-1}$, (Table 3, ref. [21], [26]). The performances of the materials prepared herein could be further improved by optimizing several parameters such as electrode and electrolyte formulation, conducting additive amount, electrolyte purity, active material particle size, etc. Nevertheless, it is important emphasizing that contrary to the toxic precursors made of phenol and formaldehyde, a green synthesis route was used to obtain our materials allowing to obtain similar performances.

The results are encouraging and demonstrate the potential application of these materials. In order to understand how materials with different properties, i.e. morphology, structure, chemical composition, interact with sodium ions, we can propose a systematic study to get more insights and improve Na ions storage in hard carbon materials in a future work.

## 4. Conclusions

A simple, eco-friendly and scalable synthesis approach to prepare hard carbons based on phenolic resins was developed in this work. Thanks to the versatility of this synthesis pathway a systematic study could be performed allowing to tune the hard carbon characteristics (yield, texture and structure) by varying the experimental parameters (i.e. solvent type, thermopolymerization and annealing temperature). As main findings we state that the solvent determines the necessary time to form the polymer resin (12 h for water and 3 days for ethanol) and influence the crosslinking which is higher when water is used as solvent, as revealed by FTIR and NMR techniques. A higher carbon yield is obtained by controlling the thermopolymerization temperature (34% at 80 °C *vs.* 22% at room temperature). The structure of the material is mainly influenced by the thermal treatment than by the chemical parameters and both d-spacing and disorder degree decrease with the increase of temperature (i.e., d-spacing decreases from 4Å at 1100 °C to 3.7Å at 1700 °C). The carbon texture could be tuned by various experimental parameters, among them, the water solvent and the thermopolymerization at room temperature induce the highest BET SSA (~80 $m^2 g^{-1}$ vs. < 10 $m^2 g^{-1}$ for the other conditions). With the increase of the temperature from 1100 °C to 1700 °C, the SSA decreases from 36 $m^2 g^{-1}$ to 3.7 $m^2 g^{-1}$. The hard carbons could be successfully used as negative electrodes for Na ions storage and promising results were obtained (270 $mAhg^{-1}$ reversible capacity). Therefore, it is possible to combine sustainable synthesis process to obtain hard carbon materials with added value for Na-ion batteries anodes.

## Acknowledgments

This work was performed in the frame of RS2E (French research network on electrochemical energy storage), ANR LABEX STOREX. The authors want to thank DGA (Direction Générale de l'Armement, grant No: 2016 60 0050) and Region Alsace (grant No: 618342) for the financial support. We also thank Dr. Luc Delmotte (NMR analysis) and Dr. Loic Vidal (HRTEM/SAED images) for technical support via IS2M technical platforms.

## Appendix A. Supplementary data

Supplementary data related to this article can be found at https://doi.org/10.1016/j.carbon.2018.06.036.

## References

[1] S. Mao, G. Lu, J. Chen, Three-dimensional graphene-based composites for energy applications, Nanoscale 7 (2015) 6924–6943, https://doi.org/10.1039/C4NR06609J.
[2] M.-S. Balogun, Y. Luo, W. Qiu, P. Liu, Y. Tong, A review of carbon materials and their composites with alloy metals for sodium ion battery anodes, Carbon 98 (2016) 162–178, https://doi.org/10.1016/j.carbon.2015.09.091.
[3] Y. Liu, B.V. Merinov, W.A. Goddard, Origin of low sodium capacity in graphite and generally weak substrate binding of Na and Mg among alkali and alkaline earth metals, Proc. Natl. Acad. Sci. Unit. States Am. 113 (2016) 3735–3739, https://doi.org/10.1073/pnas.1602473113.
[4] R.D. Shannon, Revised effective ionic radii and systematic studies of interatomic distances in halides and chalcogenides, Acta Crystallogr. A 32 (1976) 751–767, https://doi.org/10.1107/S0567739476001551.
[5] M.M. Doeff, Y. Ma, S.J. Visco, L.C.D. Jonghe, Electrochemical insertion of sodium into carbon, 1993, p. 140.
[6] J.R. Dahn, W. Xing, Y. Gao, The "falling cards model" for the structure of microporous carbons, Carbon 35 (1997) 825–830, https://doi.org/10.1016/S0008-6223(97)00037-7.
[7] E.M. Lotfabad, J. Ding, K. Cui, A. Kohandehghan, W.P. Kalisvaart, M. Hazelton, et al., High-density sodium and lithium ion battery anodes from banana peels, ACS Nano 8 (2014) 7115–7129, https://doi.org/10.1021/nn502045y.
[8] K. Hong, L. Qie, R. Zeng, Z. Yi, W. Zhang, D. Wang, et al., Biomass derived hard carbon used as a high performance anode material for sodium ion batteries, J. Mater. Chem. 2 (2014) 12733–12738, https://doi.org/10.1039/C4TA02068E.

[9] X. Meng, P.E. Savage, D. Deng, Trash to treasure: from harmful algal blooms to high-performance electrodes for sodium-ion batteries, Environ. Sci. Technol. 49 (2015) 12543–12550, https://doi.org/10.1021/acs.est.5b03882.

[10] Liming Wu, Daniel Buchholz, Christoph Vaalma, A. Giffin Guinevere, Stefano Passerini, Apple biowaste derived hard carbon as a powerful anode material for Na ion batteries, ChemElectroChem 3 (2015) 292–298, https://doi.org/10.1002/celc.201500437.

[11] T. Yang, T. Qian, M. Wang, X. Shen, N. Xu, Z. Sun, et al., A sustainable route from biomass byproduct okara to high content nitrogen-doped carbon sheets for efficient sodium ion batteries, Adv Mater Deerfield Beach Fla 28 (2016) 539–545, https://doi.org/10.1002/adma.201503221.

[12] T. Chen, L. Pan, T. Lu, C. Fu, D.H. C Chua, Z. Sun, Fast synthesis of carbon microspheres via a microwave-assisted reaction for sodium ion batteries, J. Mater. Chem. 2 (2014) 1263–1267, https://doi.org/10.1039/C3TA14037G.

[13] C. Matei Ghimbeu, J. Górka, V. Simone, L. Simonin, S. Martinet, C. Vix-Guterl, Insights on the Na+ ion storage mechanism in hard carbon: discrimination between the porosity, surface functional groups and defects, Nano Energy 44 (2018) 327–335, https://doi.org/10.1016/j.nanoen.2017.12.013.

[14] S.J.R. Prabakar, J. Jeong, M. Pyo, Nanoporous hard carbon anodes for improved electrochemical performance in sodium ion batteries, Electrochim. Acta 161 (2015) 23–31, https://doi.org/10.1016/j.electacta.2015.02.086.

[15] W. Luo, C. Bommier, Z. Jian, X. Li, R. Carter, S. Vail, et al., Low-surface-area hard carbon anode for na-ion batteries via graphene oxide as a dehydration agent, ACS Appl. Mater. Interfaces 7 (2015) 2626–2631, https://doi.org/10.1021/am507679x.

[16] Y. Li, Z. Wang, L. Li, S. Peng, L. Zhang, M. Srinivasan, et al., Preparation of nitrogen- and phosphorous co-doped carbon microspheres and their superior performance as anode in sodium-ion batteries, Carbon 99 (2016) 556–563, https://doi.org/10.1016/j.carbon.2015.12.066.

[17] G. Hasegawa, K. Kanamori, N. Kannari, J. Ozaki, K. Nakanishi, T. Abe, Studies on electrochemical sodium storage into hard carbons with binder-free monolithic electrodes, J. Power Sources 318 (2016) 41–48, https://doi.org/10.1016/j.jpowsour.2016.04.013.

[18] C. Jo, Y. Park, J. Jeong, K.T. Lee, J. Lee, Structural effect on electrochemical performance of ordered porous carbon electrodes for Na-Ion batteries, ACS Appl. Mater. Interfaces 7 (2015) 11748–11754, https://doi.org/10.1021/acsami.5b03186.

[19] W. Luo, J. Schardt, C. Bommier, B. Wang, J. Razink, J. Simonsen, et al., Carbon nanofibers derived from cellulose nanofibers as a long-life anode material for rechargeable sodium-ion batteries, J. Mater. Chem. 1 (2013) 10662–10666, https://doi.org/10.1039/C3TA12389H.

[20] Zhang B, Ghimbeu CM, Laberty C, Vix-Guterl C, Tarascon J-M. Correlation between microstructure and Na storage behavior in hard carbon. Adv Energy Mater n.d.;6:1501588. doi:10.1002/aenm.201501588.

[21] Y. Li, L. Mu, Y.-S. Hu, H. Li, L. Chen, X. Huang, Pitch-derived amorphous carbon as high performance anode for sodium-ion batteries, Energy Storage Mater 2 (2016) 139–145, https://doi.org/10.1016/j.ensm.2015.10.003.

[22] Z. Yuan, L. Si, X. Zhu, Three-dimensional hard carbon matrix for sodium-ion battery anode with superior-rate performance and ultralong cycle life, J. Mater. Chem. 3 (2015) 23403–23411, https://doi.org/10.1039/C5TA07223A.

[23] H. Wang, Z. Shi, J. Jin, C. Chong, C. Wang, Properties and sodium insertion behavior of Phenolic Resin-based hard carbon microspheres obtained by a hydrothermal method, J. Electroanal. Chem. 755 (2015) 87–91, https://doi.org/10.1016/j.jelechem.2015.07.032.

[24] J. Ye, J. Zang, Z. Tian, M. Zheng, Q. Dong, Sulfur and nitrogen co-doped hollow carbon spheres for sodium-ion batteries with superior cyclic and rate performance, J. Mater. Chem. 4 (2016) 13223–13227, https://doi.org/10.1039/C6TA04592H.

[25] Hasegawa G, Kanamori K, Kannari N, Ozaki J, Nakanishi K, Abe T. Hard carbon anodes for Na-Ion batteries: toward a practical use. ChemElectroChem n.d.;2:1917–1920. doi:10.1002/celc.201500412.

[26] H. Zhang, H. Ming, W. Zhang, G. Cao, Y. Yang, Coupled carbonization strategy toward advanced hard carbon for high-energy sodium-ion battery, ACS Appl. Mater. Interfaces 9 (2017) 23766–23774, https://doi.org/10.1021/acsami.7b05687.

[27] C.M. Ghimbeu, L. Vidal, L. Delmotte, J.-M.L. Meins, C. Vix-Guterl, Catalyst-free soft-template synthesis of ordered mesoporous carbon tailored using phloroglucinol/glyoxylic acid environmentally friendly precursors, Green Chem. 16 (2014) 3079–3088, https://doi.org/10.1039/C4GC00269E.

[28] I.P. Singh, J. Sidana, S.B. Bharate, W.J. Foley, Phloroglucinol compounds of natural origin: synthetic aspects, Nat. Prod. Rep. 27 (2010) 393–416, https://doi.org/10.1039/B914364P.

[29] G. Moussa, C. Matei Ghimbeu, P.-L. Taberna, P. Simon, C. Vix-Guterl, Relationship between the carbon nano-onions (CNOs) surface chemistry/defects and their capacitance in aqueous and organic electrolytes, Carbon 105 (2016) 628–637, https://doi.org/10.1016/j.carbon.2016.05.010.

[30] C. Nita, M. Bensafia, C. Vaulot, L. Delmotte, C. Matei Ghimbeu, Insights on the synthesis mechanism of green phenolic resin derived porous carbons via a salt-soft templating approach, Carbon 109 (2016) 227–238, https://doi.org/10.1016/j.carbon.2016.08.011.

[31] E.R. Buiel, A.E. George, J.R. Dahn, Model of micropore closure in hard carbon prepared from sucrose, Carbon 37 (1999) 1399–1407, https://doi.org/10.1016/S0008-6223(98)00335-2.

[32] M. Sopronyi, F. Sima, C. Vaulot, L. Delmotte, A. Bahouka, C. Matei Ghimbeu, Direct synthesis of graphitic mesoporous carbon from green phenolic resins exposed to subsequent UV and IR laser irradiations, Sci. Rep. (2016) 6, https://doi.org/10.1038/srep39617.

[33] C.M. Ghimbeu, M. Sopronyi, F. Sima, L. Delmotte, C. Vaulot, C. Zlotea, et al., One-pot laser-assisted synthesis of porous carbon with embedded magnetic cobalt nanoparticles, Nanoscale 7 (2015) 10111–10122, https://doi.org/10.1039/C5NR01687H.

[34] T.-H. Ko, W.-S. Kuo, Y.-H. Chang, Raman study of the microstructure changes of phenolic resin during pyrolysis, Polym. Compos. 21 (2000) 745–750, https://doi.org/10.1002/pc.10229.

[35] D.A. Stevens, J.R. Dahn, The mechanisms of lithium and sodium insertion in carbon materials, J. Electrochem. Soc. 148 (2001) A803–A811, https://doi.org/10.1149/1.1379565.

[36] C. Bommier, D. Mitlin, X. Ji, Internal structure – Na storage mechanisms – electrochemical performance relations in carbons, Prog. Mater. Sci. 97 (2018) 170–203, https://doi.org/10.1016/j.pmatsci.2018.04.006.

[37] M. Sawicki, L.L. Shaw, Advances and challenges of sodium ion batteries as post lithium ion batteries, RSC Adv. 5 (2015) 53129–53154, https://doi.org/10.1039/C5RA08321D.